JACS
JOURNAL OF THE AMERICAN CHEMICAL SOCIETY
pubs.acs.org/JACS
Article

Self-adaptive Metal–Organic Framework Assembles Di-iron Active Sites to Mimic Monooxygenases

Zitong Wang, Pierce Yeary, Xuanyu Feng, and Wenbin Lin*

Cite This: J. Am. Chem. Soc. 2023, 145, 8647–8655
Read Online

ABSTRACT: Despite significant efforts, it remains a challenge to design artificial enzymes that can mimic both structures and functions of natural enzymes. Here, we report the post-synthetic construction of binuclear iron catalysts in MOF-253 to mimic natural di-iron monooxygenases. The adjacent bipyridyl (bpy) linkers in MOF-253 can freely rotate to form the $[(bpy)Fe^{III}(\mu_2\text{-}OH)]_2$ active site in a self-adaptive fashion. The composition and structure of the $[(bpy)Fe^{III}(\mu_2\text{-}OH)]_2$ active sites in MOF-253 were characterized by a combination of inductively coupled plasma–mass spectrometry, thermogravimetric analysis, X-ray absorption spectrometry, and Fourier-transform infrared spectroscopy. The MOF-based artificial monooxygenase effectively catalyzed oxidative transformations of organic compounds, including C–H oxidation and alkene epoxidation reactions, using O_2 as the only oxidant, which indicates the successful recapitulation of the structure and functions of natural monooxygenases using readily accessible MOFs. The di-iron system exhibited at least 27 times higher catalytic activity than the corresponding mononuclear control. DFT calculations showed that the binuclear system had a 14.2 kcal/mol lower energy barrier than the mononuclear system in the rate-determining C–H activation process, suggesting the importance of cooperativity of the iron centers in the $[(bpy)Fe^{III}(\mu_2\text{-}OH)]_2$ active site in the rate-determining step. The stability and recyclability of the MOF-based artificial monooxygenase were also demonstrated.

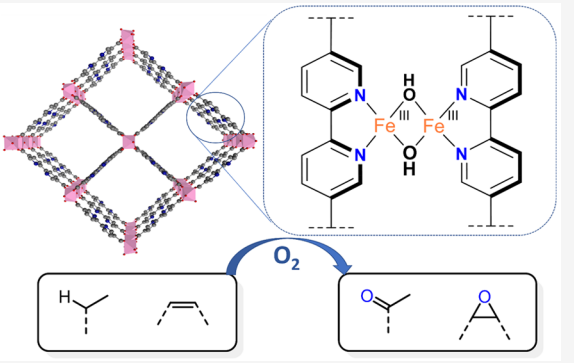

INTRODUCTION

Natural enzymes play crucial roles in the metabolism of xenobiotics and realize important chemical transformations with extraordinary efficiency and selectivity. Monooxygenases are one important class of natural enzymes that can insert one oxygen atom into substrates utilizing molecular oxygen with the aid of sacrificial reductants such as NADH (NAD = nicotinamide adenine dinucleotide). Monooxygenases can be divided into several categories, including heme-based, flavin-based, and other non-heme-based enzymes.[1−9] Among them, non-heme monooxygenases with binuclear active sites efficiently activate O_2 through multielectron processes without forming high-valent terminal metal oxo species due to the synergy between the two metal centers. One example is the hydroxylase (MMOH) component of soluble methane monooxygenase (sMMO), which catalyzes the transformation of methane to methanol in methanotrophs.[10−16]

Over the past few decades, many synthetic model complexes have been prepared to mimic monooxygenases, but few of them can efficiently catalyze oxidative transformations of organic compounds.[17−22] H_2O_2 and other expensive oxidants such as TEMPO [(2,2,6,6-tetramethylpiperidin-1-yl)oxyl] are often needed in these model reactions, while cheaper and more environmentally friendly O_2 seldom worked as the oxidant.[23−25] Few of these synthetic models are based on binuclear centers due to the difficulty in their synthesis. Stoichiometric amounts of these model complexes are often needed for oxidative transformations such as hydroxylation or epoxidation reactions.

Constructed from metal cluster secondary building units (SBUs) and organic linkers, metal–organic frameworks (MOFs) have attracted significant attention due to their crystalline structures, high porosity, and molecular tunability. In the past few years, many MOF catalysts have been developed by incorporating catalytic species into SBUs or linkers, leading to extraordinary catalytic efficiency.[26−35]

Building on these successes, recent efforts have been extended to designing MOF-based artificial enzymes for CO_2 reduction, monooxygenation with O_2, and other important reactions.[36−49] In particular, a dicopper system has been built on the SBUs of a Ti-MOF to mimic the structures and functions of monooxygenases (Figure 1).[36] However, these SBU-based monooxygenase mimics do not allow the incorporation of nitrogen-based ligands which play crucial

Received: February 9, 2023
Published: April 6, 2023

https://doi.org/10.1021/jacs.3c01498
J. Am. Chem. Soc. 2023, 145, 8647–8655

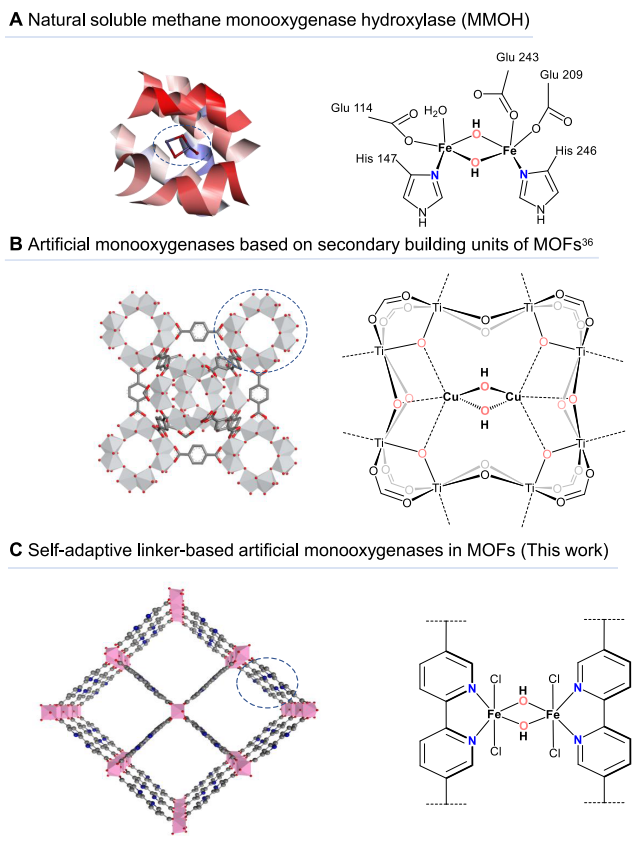

Figure 1. Binuclear catalytic centers in natural monooxygenases and MOF-based artificial monooxygenases.

roles in natural enzymes. Dual-atom catalytic centers have been engineered in other heterogeneous systems to enhance oxygen evolution and reduction processes.[50−54] In this work, we report a self-adaptive nitrogen-based ligand system in MOF-253 for the design of a $[Fe^{III}(\mu_2\text{-OH})]_2$ artificial monooxygenase. The parallel arrangement and suitable distance between the bipyridine linkers in MOF-253 allow for the efficient construction of monooxygenase-mimicking binuclear $[(bpy)\text{-}Fe^{III}(\mu_2\text{-OH})]_2$ catalytic centers (Figure 1C). This di-iron system exhibits high catalytic activities toward C−H oxidation and epoxidation reactions with O_2 as the oxidant. The present work highlights the potential of using linkers in MOFs as self-adaptive ligand systems to construct artificial enzymes with binuclear catalytic centers.

RESULTS AND DISCUSSION

Synthesis and Characterization of MOF-Based Di-iron Artificial Monooxygenase. The di-iron artificial monooxygenase and its mononuclear analogue were rationally constructed within MOF-253, an aluminum-based MOF. 2,2′-Bipyridine-5,5′-dicarboxylate (bpydc) serves as the linker to connect two oxophilic Al^{3+} ions via the carboxylate groups, leaving soft bipyridine sites for the insertion of the catalytic iron center via post-synthetic modification (PSM). The six-coordinated Al^{3+} cations are also bridged by hydroxides to form one-dimensional chains, and the bpydc linkers are arranged in parallel to each other to give rhombic channels. The distance between two adjacent bpydc linkers is about 6.6 Å, and the free rotation of the bpydc linkers allows them to self-adaptively connect two iron centers with μ_2-OH groups to mimic natural binuclear monooxygenases.

MOF-253 was synthesized through solvothermal reactions between $Al(NO_3)_3{\cdot}9H_2O$ and H_2bpydc (Figure 2A).[55−59] Powder X-ray diffraction (PXRD) studies demonstrated the synthesis of MOF-253 as crystalline white powders, and thermal gravimetric analysis (TGA) supported the chemical formula of Al(OH) (bpydc) (Figure S2). The treatment of MOF-253 with $FeCl_2$ in tetrahydrofuran afforded the pre-catalyst **1-pre**, which was suspended in methanol and oxidized under an O_2 atmosphere to give the MOF catalyst **1** (Figure

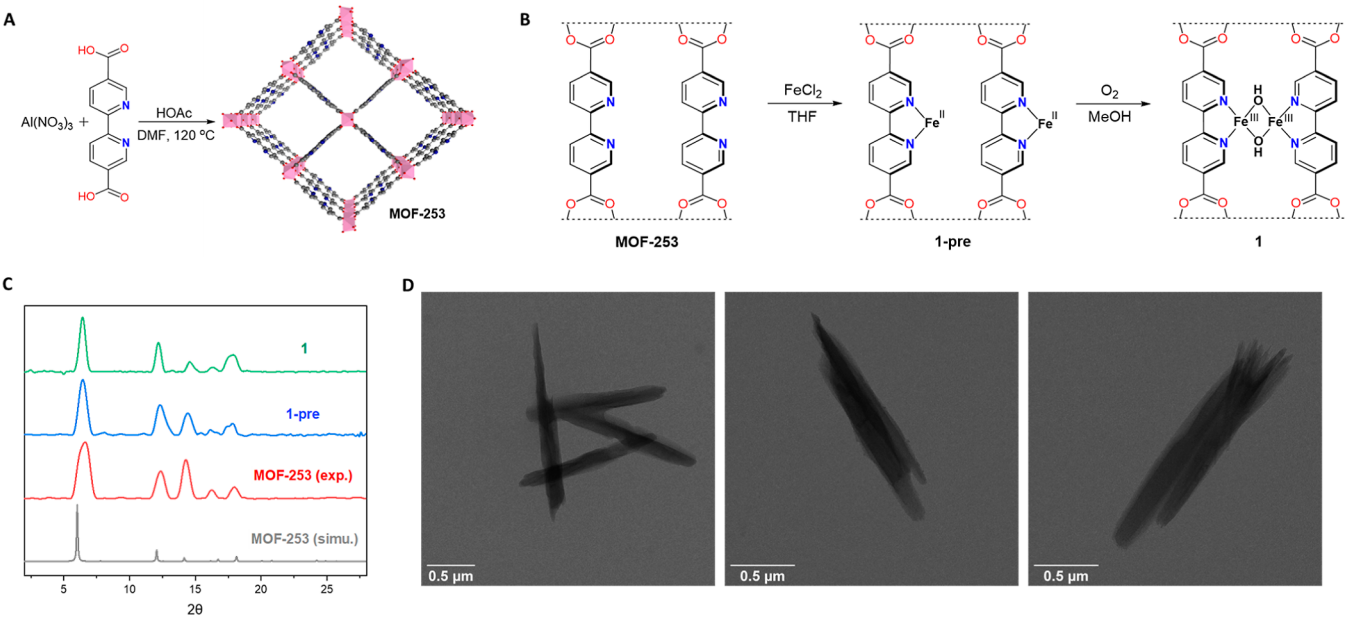

Figure 2. A) Synthetic scheme of MOF-253. (B) Post-synthetic modification of MOF-253 to construct $[(bpy)Fe(\mu_2\text{-OH})]_2$ catalytic centers. (C) PXRD patterns of MOF-253 (red), **1-pre** (blue), and **1** (green) along with the simulated pattern for MOF-253. (D) TEM images of MOF-253 (left), **1-pre** (middle), and **1** (right).

https://doi.org/10.1021/jacs.3c01498
J. Am. Chem. Soc. 2023, 145, 8647−8655

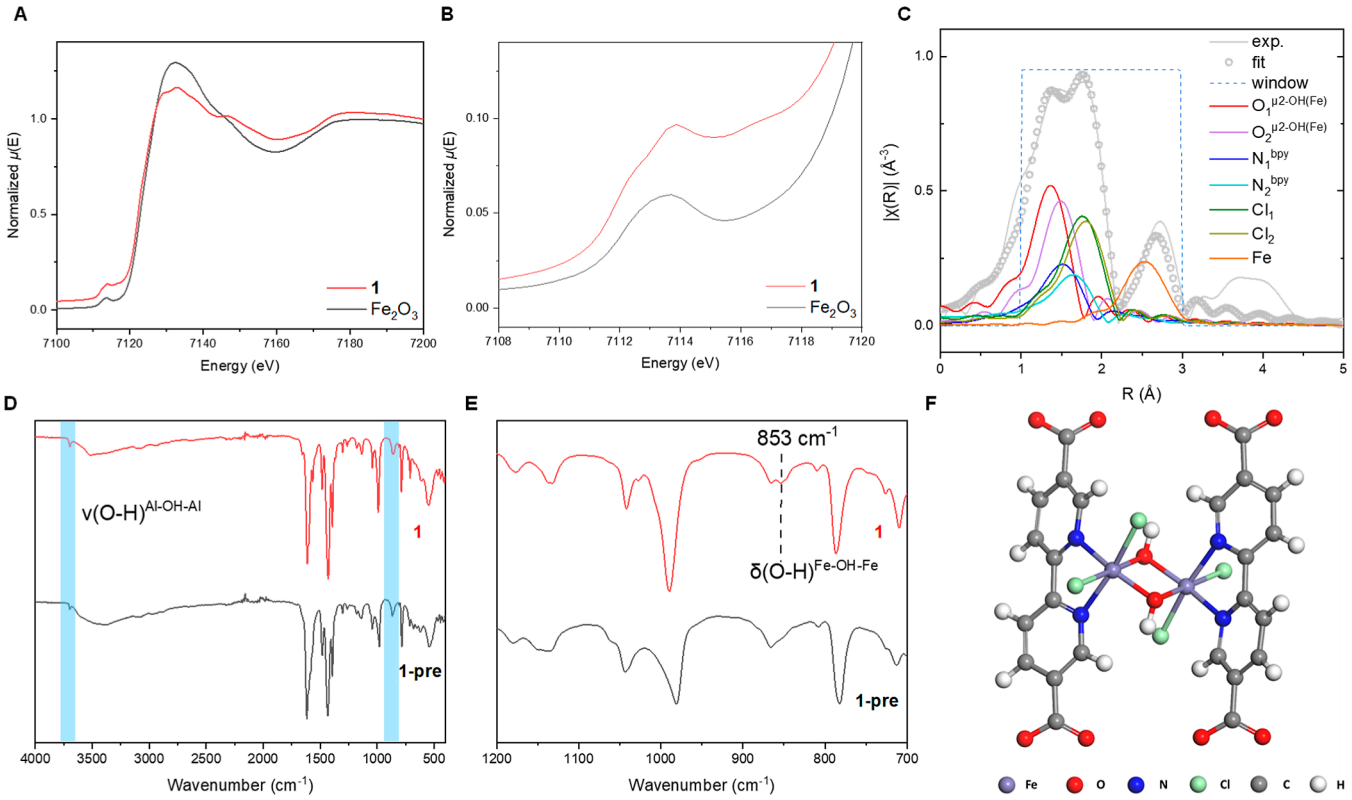

Figure 3. A) Normalized Fe K-edge XAS spectra of the XANES region of **1** (red line) and Fe_2O_3 (gray line). (B) Pre-edge region at 7108−7120 eV corresponding to the 1s-to-3d transition of Fe^{III}. (C) EXAFS spectrum and fit in R-space at Fe K-edge of **1** as well as contribution of different scatterers. (D) Full IR spectra of **1-pre** (gray) and **1** (red). (E) Generation of a new peak at 853 cm^{-1} after oxidation. (F) Structural model of the local coordination environment of the di-iron center in **1**.

Table 1. C−H Oxidation of Indane Catalyzed by 1 and Controls

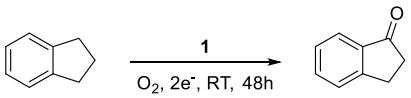

entry	deviation from standard conditions[a]	yield
1	no deviation	80%
2	no catalyst	no reaction
3	MOF-253 as the catalyst[b]	1%
4	N_2 atmosphere instead of O_2	No reaction
5	no sacrificial reagent	No reaction
6	0.5 mol % of mononuclear control (2) as the catalyst	3%

[a]Standard conditions: 0.5 mol % **1** was used as the catalyst. 5 equiv of ^{t}BuCHO was added in five portions as a sacrificial reductant. The reaction lasted for 48 h with an O_2 balloon. The yield was determined by GC−MS. [b]1.0 mg of MOF-253 was used.

2B). It was proposed that two adjacent Fe^{II} centers in **1-pre** were oxidized to Fe^{III} centers to form the $[(bpy)Fe^{III}(\mu_2\text{-}OH)]_2$ catalytic centers. The color of the MOF suspension changed from dark gray to yellow upon aerobic oxidation, suggesting the change of the oxidation state and coordination environment of iron centers. Inductively coupled plasma−mass spectrometry (ICP−MS) analysis showed a 1:0.89 Al-to-Fe molar ratio, indicating nearly complete occupation of bpy sites by iron centers and a high percentage of di-iron pairs in the MOF. TGA analysis supported the chemical composition of **1-pre** and **1** (Figure S4). PXRD studies showed that the crystallinity of the MOF was retained during Fe^{II} installation and aerobic oxidation processes (Figure 2C). Transmission electron microscopy (TEM) indicated that the MOF maintained a rod-like morphology of ∼0.1 μm in diameter and ∼1 μm in length throughout the PSM processes (Figure 2D).

To further elucidate the effect of di-iron centers on O_2 activation, mononuclear catalyst **2** was also synthesized. MOF-253-$(bpy)_{0.1}$ was solvothermally synthesized using a 9:1 ratio of 4,4′-biphenyldicarboxylic acid (H_2bpdc) and H_2bpydc as linkers. ^{1}H NMR spectroscopy of the digested MOF showed an 11% bpydc loading (Figure S6). MOF-253-$(bpy)_{0.1}$ showed the same PXRD pattern as MOF-253 (Figure S7). The mononuclear catalyst **2** was obtained using the same PSM procedures as for **1**, with an Al/Fe molar ratio of 1:0.10 as determined by ICP−MS. In **2**, the di-iron centers are statistically estimated to be less than 1% of all iron sites.

Identification of Binuclear $[(bpy)Fe^{III}(\mu_2\text{-}OH)]_2$ Catalytic Centers. We performed Fe K-edge X-ray absorption near-edge structure (XANES) and extended X-ray absorption fine structure (EXAFS) analyses of **1** to demonstrate the presence of binuclear catalytic centers, which are the active sites in the oxidized form of soluble methane monooxygenase hydroxylase (sMMOH). The Fe K-edge energy of **1** was found to be 7122.9 eV (Figure 3A), which is similar to the value of Fe_2O_3 (7122.4 eV). Furthermore, similar to previously reported six-coordinated Fe complexes, **1** showed a pre-edge peak at 7111−7115 eV with low density (Figure 3B), attributable to the spin-forbidden 1s-to-3d transition of Fe^{3+} ions.[60−62] These results indicate the presence of six-coordinate Fe^{3+} centers with an octahedral geometry in **1**.

https://doi.org/10.1021/jacs.3c01498
J. Am. Chem. Soc. 2023, 145, 8647−8655

Table 2. C−H Oxidation (Entries 1−5)[a] and Epoxidation (Entries 6−13)[b] Reactions Catalyzed by 1

Entry	Substrate	Catalyst Loading	Product	Conversion (Yield)	TON	Entry	Substrate	Catalyst Loading	Product	Conversion (Yield)	TON
1		0.5 mol%		88% (78%)	156	8		0.2 mol%		100% (98%)	490
2		0.25 mol%		95% (73%)	292	9		0.2 mol%		99% (86%)	470
3		0.5 mol%		45% (40%)	80	10		0.5 mol%		89% (80%)	160
4		0.5 mol%		100% (78%)	156	11	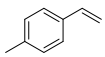	0.5 mol%	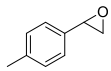	82% (70%)	140
5		0.5 mol%		97% (75%)	150	12	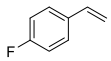	0.5 mol%	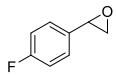	64% (57%)	114
6		0.2 mol%		100% (92%)	460	13	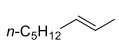	0.5 mol%	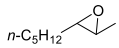	89% (88%)	176
7		0.2 mol%		100% (97%)	485						

[a]Standard conditions: the reactions were performed with 1 as the catalyst and 5 equiv. of ^{t}BuCHO added in five portions (2.5 equiv for entry 2) with an O_2 balloon over 48 h. Conversions were determined by GC−MS before product purification, and yields were determined after the isolation of products by column chromatography. [b]Standard conditions: the reactions were performed with 1 and 2 equiv of ^{t}BuCHO with an O_2 balloon over 24 h. The conversions and yields were determined by GC−MS.

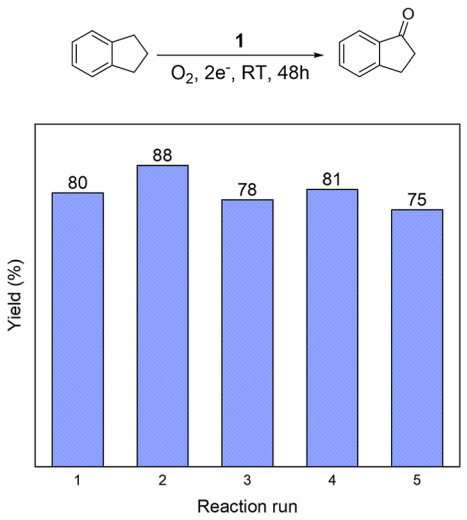

Figure 4. Recovery and reuse of 1 in catalytic C−H oxidation of indane.

Density functional theory (DFT) calculations were performed with the B3LYP functional to determine the local coordination environment of Fe centers in 1. DFT calculations showed a distorted octahedral geometry for 1, with each Fe center coordinating to two N atoms of bpydc, two Cl atoms, and two μ_2-OH groups. The lengths of Fe−N, Fe−Cl, and Fe−O bonds were calculated to be 2.02/2.17, 2.24/2.28, and 1.87/1.98 Å, respectively, and the Fe−Fe distance was calculated to be 2.93 Å.

The coordination environments of the Fe centers in 1 were probed by EXAFS (Figure 3C,F). 1 showed strong Fe−O and Fe−Fe single scattering signals, suggesting the presence of a $[Fe^{III}(\mu_2\text{-OH})]_2$ moiety. Fitting of EXAFS data with the DFT-optimized structure model revealed Fe−N, Fe−Cl, and Fe−O bond lengths of 2.02/2.17, 2.24/2.28, and 1.87/1.99 Å, respectively, and an Fe−Fe distance of 2.93 Å. These bond lengths and Fe−Fe distances agree well with those from DFT calculations. The Fe−Fe distance is also consistent with the previously reported values for natural di-iron enzymes and synthetic models of binuclear monooxygenases.

Infrared spectra of 1 and **1-pre** were also compared to support the presence of the bridging μ_2-OH group. Both **1-pre** and 1 showed a sharp peak at 3696 cm^{-1}, which was assigned to be υ(O−H) of the μ_2-OH between the two Al centers of MOF-253 (Figure 3D).[55,63] After oxidation, a new peak appeared at 853 cm^{-1} (Figure 3E), which was consistent with the reported δ(O−H) frequency of μ_2-OH groups between two Fe centers.[64,65] This result supports the generation of μ_2-OH groups upon aerobic oxidation of **1-pre** to 1.

Monooxygenation Reactions with O_2. With sacrificial reductants such as NADH, natural monooxygenases catalyze C−H bond oxidation with cheap and environmentally friendly O_2. With $[(bpy)Fe^{III}(\mu_2\text{-OH})]_2$ catalytic centers, 1 efficiently catalyzed the C−H oxidation reaction of various substrates using O_2 as the only oxidant.

We used the C−H oxidation of indane as the model reaction for reaction condition optimization. With 1 as the catalyst, indane was oxidized by O_2 to give 1-indanol, which was further oxidized to generate 1-indanone as the final product.[36,66,67] Screening of different solvents identified acetonitrile as the best solvent for indane oxidation (Table S2). The reactions in other polar solvents such 1,2-dichloroethane (DCE) and benzotrifluoride produced 1-indanone in lower yields, and the

https://doi.org/10.1021/jacs.3c01498
J. Am. Chem. Soc. 2023, 145, 8647−8655

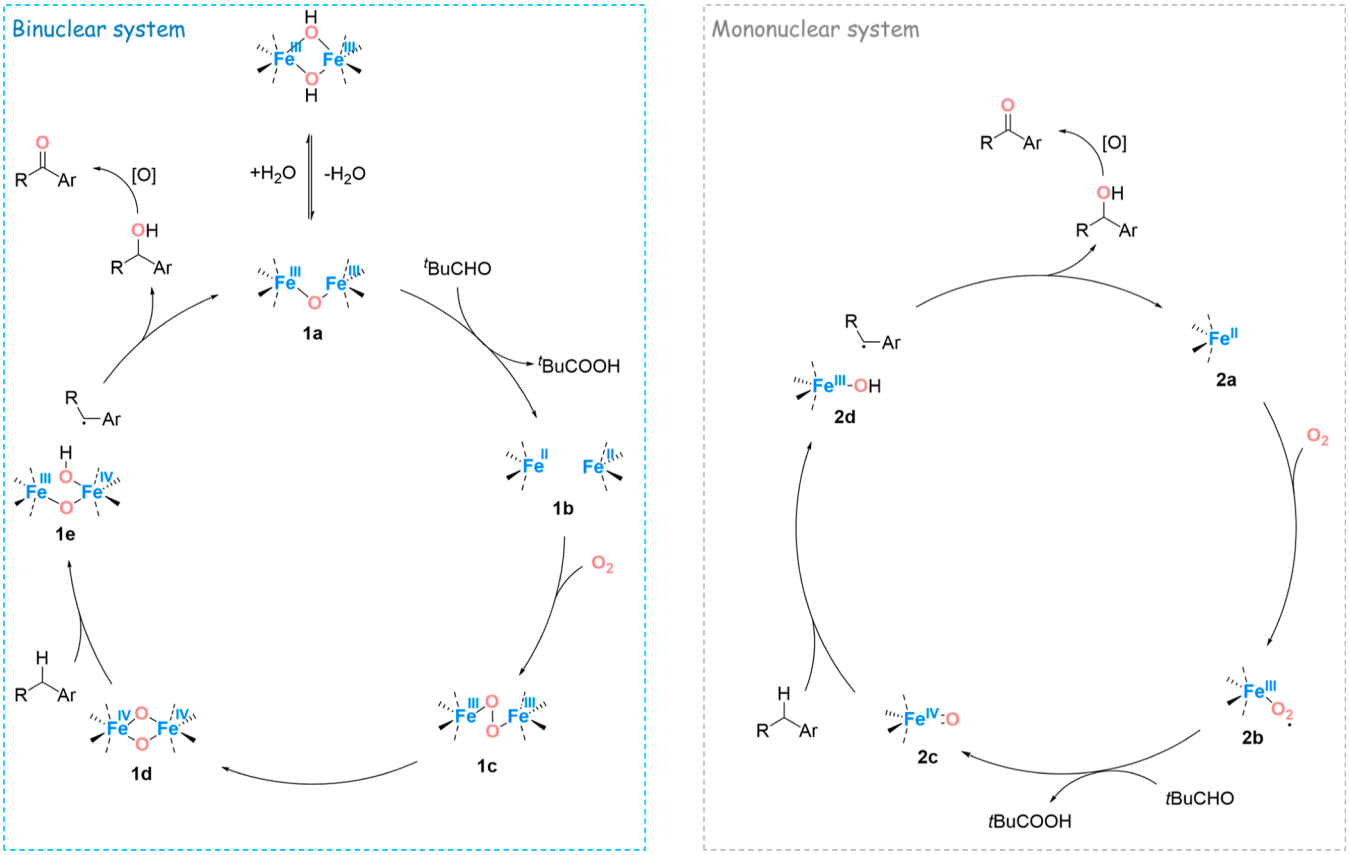

Figure 5. Proposed mechanisms for C−H oxidation reactions by binuclear (left) and mononuclear (right) iron catalysts.

reactions in non-polar solvents such as *n*-hexane failed to yield 1-indanone. The choice of sacrificial reductants also had a significant influence on the oxidation reaction (Table S3). Pivaldehyde (^{t}BuCHO) was superior to other reductants such as cyclohexanecarbaldehyde, L-ascorbic acid, and *N*-benzyl-1,4-dihydronicotinate. We also found that the addition of 5 equivalents of ^{t}BuCHO in five portions further increased the 1-indanone yield when compared to the addition of the same amount of ^{t}BuCHO in a single portion. This phenomenon can be explained by the unproductive self-oxidation and quenching of excess ^{t}BuCHO, which adversely competes with the desired substrate oxidation. Decreasing the catalyst loading from 10 to 0.5 mol % (based on Fe) did not affect the reaction yield, indicating a high efficiency of the MOF catalyst due to its efficient mass transfer (through large pores and channels) and high catalyst stability (as a result of active site isolation) (Figure S8).

In the optimized protocol, an alkane substrate was dissolved in acetonitrile with suspended **1**, followed by the addition of ^{t}BuCHO as a sacrificial reductant in five portions over 48 h. An O_2 balloon was attached to the reactor to provide the oxygen source. Under this condition, indane was converted to 1-indanone in 80% yield. 3% of 1-indanol and 5% of over-oxidized products were also obtained. In comparison, the oxidation reaction with the mononuclear catalyst **2** gave 1-indanone in 3% yield under the same condition (Table 1), resulting in a 27-fold difference between the catalytic activities of **1** and **2**. The di-iron system thus showed much enhanced catalytic activity over the mononuclear system. The substrate scope of C−H oxidation reaction was also examined; several compounds with benzylic C−H bonds at their α positions were readily oxidized to the desired ketone products with high efficiency (entries 1−5, Table 2).

We also performed catalyst recovery and reuse experiments to evaluate the stability of the MOF catalyst. **1** was recovered by centrifugation from the reaction mixture and used in five consecutive runs of indane C−H oxidation. There was no significant decrease of catalytic performance during the five runs, illustrating the high stability of this MOF-based di-iron system under the reaction conditions (Figure 4). ICP−MS analysis showed the leaching of 1.5% Fe and 0.5% Al after the first reaction, supporting the stability of **1**.

Natural monooxygenases also catalyze the insertion of one oxygen atom into the C−C double bond to generate epoxides using O_2 as the oxidant. We tested the epoxidation of a range of alkenes with O_2 in the presence of **1** as an artificial monooxygenase. **1** efficiently catalyzed epoxidation reactions of a variety of substrates, including cyclic and linear alkenes as well as styrene derivatives. The epoxides were obtained in high yields at room temperature and under an atmospheric pressure of O_2 over 24 h (entries 6−13, Table 2).

DFT Calculations of C−H Oxidation Energy Profiles. Based on the well-established mechanisms of dioxygen and C−H activation by natural monooxygenases such as sMMOH, Rieske oxygenases, and cytochrome P450, we propose the catalytic processes of binuclear and mononuclear systems in Figure 5. As the resting state of the catalyst, a $[Fe^{III}(\mu_2\text{-}OH)]_2$ center can reversibly lose water to generate the $[Fe^{III}{}_2(\mu_2\text{-}O)]$ species (**1a**), which is reduced by the sacrificial reductant to give the di-iron catalyst **1b** with two unbridged Fe^{II} centers. Similar to the reduced form of sMMOH, the two Fe^{II} centers in **1b** activate O_2 to sequentially form $[Fe^{III}{}_2(\mu_2\text{-}O_2)]$ (**1c**) and

https://doi.org/10.1021/jacs.3c01498
J. Am. Chem. Soc. 2023, 145, 8647−8655

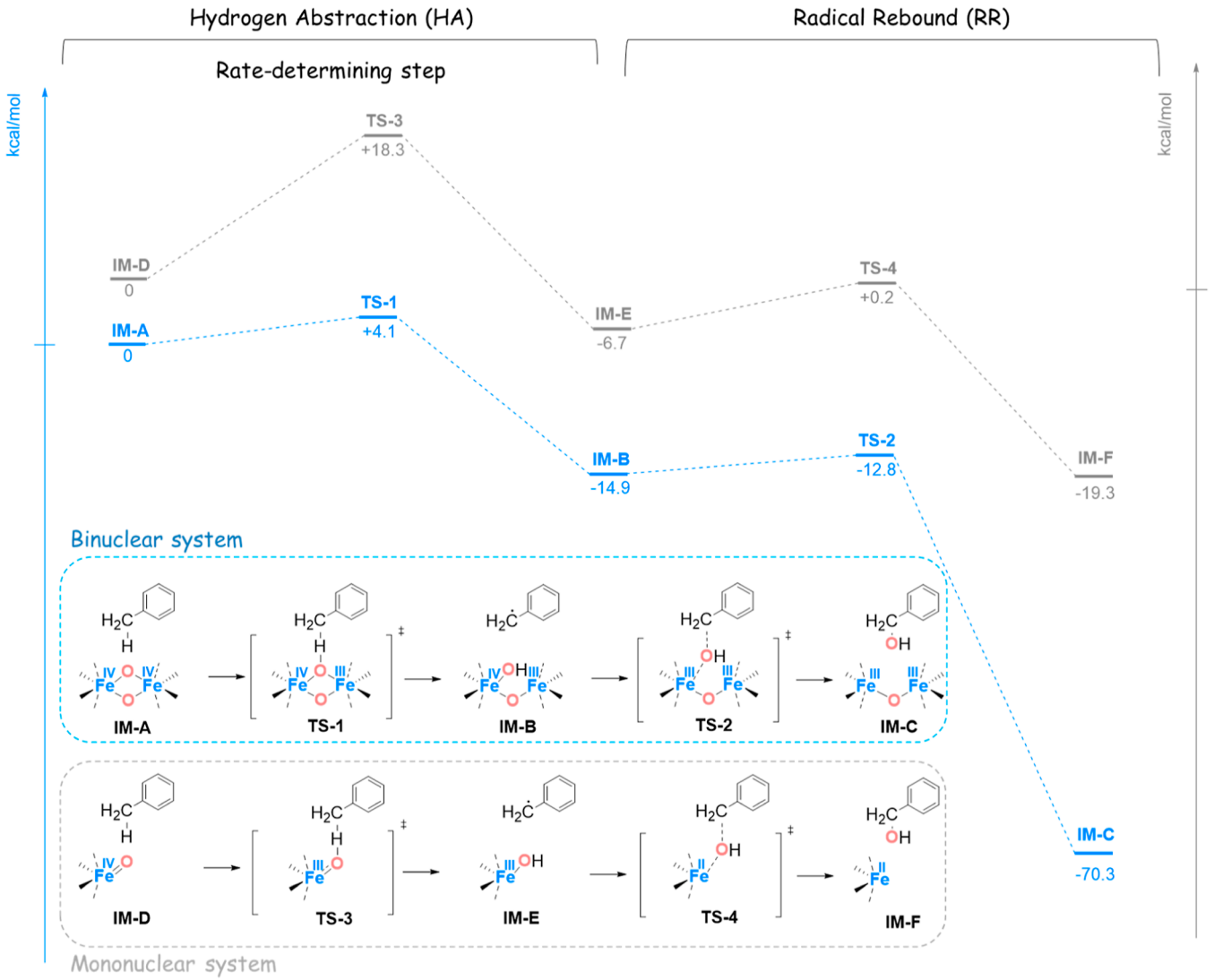

Figure 6. DFT-calculated energy profiles of C−H activation processes catalyzed by binuclear and mononuclear systems.

$[Fe^{IV}(\mu_2\text{-}O)]_2$ (**1d**) species. Spectroscopic and kinetic studies have thoroughly characterized such bridging peroxo- and oxo-di-iron intermediates in enzyme-catalyzed monooxygenation reactions, which are known as intermediates P and Q, respectively. With the synergy of two Fe centers, the O═O bond can be easily cleaved.

For the mononuclear system, the sacrificial reductant is required in the dioxygen activation process to provide electrons for the cleavage of the O═O bond, giving the Fe^{IV} intermediate **2c** with a terminal oxo group. **2c** cleaves the C−H bond of the substrate via a hydrogen abstraction (HA) step to form the Fe^{III}−OH intermediate **2d** and a carbon radical. This reactive carbon radical further undergoes radical rebound to release the corresponding alcohol, which is further oxidized to ketone as the final product. The Fe centers are simultaneously converted back to the initial state of **2a**.

In enzyme-catalyzed monooxygenation reactions, kinetic experiments and theoretical studies have shown the hydrogen abstraction (HA) step as the rate-determining step.[68,69] We carried out DFT calculations on the C−H activation processes (including hydrogen abstraction and radical rebound steps) of both binuclear and mononuclear systems to rationalize the superior catalytic performance of the di-iron catalyst **1** over its mononuclear analogue **2** (Figure 6). The calculations showed that the di-iron-catalyzed hydrogen abstraction step is associated with a very small energy barrier (4.1 kcal/mol), which is 14.2 kcal/mol lower than that of the mononuclear pathway (18.3 kcal/mol). For both binuclear and mononuclear systems, the subsequent radical rebound step has very small energy barriers of 2.1 and 4.5 kcal/mol, respectively. The radical rebound step is thermodynamically favorable and unlikely to be rate-limiting. The two Fe^{IV} centers in **1d** thus cooperatively abstract hydrogen from the substrate to significantly reduce the energy barrier of the rate-determining step, leading to the superior catalytic monooxygenation activity of binuclear catalyst **1** to that of the mononuclear catalyst **2**.

CONCLUSIONS

In this work, we report the construction of biomimicking di-iron active sites in the Al-based MOF-253 in a self-adaptive fashion. With an appropriate distance, the two adjacent Fe-coordinated bipyridine linkers in MOF-253 freely rotate to assemble $[(bpy)Fe^{III}(\mu_2\text{-}OH)]_2$ active sites. The binuclear Fe sites in the MOF mimic natural monooxygenases to catalyze C−H oxidation and alkene epoxidation reactions with wide substrate scopes at room temperature, using atmospheric O_2 as

https://doi.org/10.1021/jacs.3c01498
J. Am. Chem. Soc. 2023, 145, 8647−8655

the only oxidant. The MOF-based binuclear Fe catalyst showed 27 times higher catalytic activity than its mononuclear control. DFT calculations showed that the binuclear system had a 14.3 kcal/mol lower energy barrier in the rate-determining hydrogen abstraction step than the mononuclear control, which not only accounts for the drastic difference in their catalytic performances but also suggests the importance of cooperativity between Fe centers on the rate-determining C−H activation process. The MOF-based di-iron catalyst was recovered after the monooxygenation reaction and used in at least five runs of reactions with no deterioration in the catalytic performance. This work highlights the potential of using self-adaptive MOFs for the construction of robust binuclear catalytic sites to mimic the structures and functions of natural enzymes.

■ ASSOCIATED CONTENT

Supporting Information

The Supporting Information is available free of charge at https://pubs.acs.org/doi/10.1021/jacs.3c01498.

Synthesis and characterization of MOF-253, **1-pre**, **1**, and other control groups; reaction procedures and characterization results of reaction products; and DFT calculations (PDF)

■ AUTHOR INFORMATION

Corresponding Author

Wenbin Lin − *Department of Chemistry, The University of Chicago, Chicago, Illinois 60637, United States;* orcid.org/0000-0001-7035-7759; Email: wenbinlin@uchicago.edu

Authors

Zitong Wang − *Department of Chemistry, The University of Chicago, Chicago, Illinois 60637, United States;* orcid.org/0000-0001-7883-5276

Pierce Yeary − *Department of Chemistry, The University of Chicago, Chicago, Illinois 60637, United States*

Xuanyu Feng − *Department of Chemistry, The University of Chicago, Chicago, Illinois 60637, United States;* orcid.org/0000-0003-1355-1445

Complete contact information is available at: https://pubs.acs.org/10.1021/jacs.3c01498

Notes

The authors declare no competing financial interest.

■ ACKNOWLEDGMENTS

We thank Yingjie Fan for experimental help. This work was supported by NSF (CHE-2102554) and the University of Chicago. XAS analysis was performed at Beamline 10-BM, supported by the Materials Research Collaborative Access Team (MRCAT). Use of the Advanced Photon Source, an Office of Science User Facility operated for the U.S. DOE Office of Science by ANL, was supported by the U.S. DOE under the contract DE-AC02-06CH11357.

■ REFERENCES

(1) Cao, Y.; Li, X.; Ge, J. Enzyme Catalyst Engineering toward the Integration of Biocatalysis and Chemocatalysis. *Trends Biotechnol.* **2021**, *39*, 1173−1183.

(2) Wong, C.-H. Enzymatic Catalysts in Organic Synthesis. *Science* **1989**, *244*, 1145−1152.

(3) Sheldon, R. A.; Woodley, J. M. Role of Biocatalysis in Sustainable Chemistry. *Chem. Rev.* **2018**, *118*, 801−838.

(4) Que, L.; Tolman, W. B. Biologically inspired oxidation catalysis. *Nature* **2008**, *455*, 333−340.

(5) Eswaramoorthy, S.; Bonanno, J. B.; Burley, S. K.; Swaminathan, S. Mechanism of action of a flavin-containing monooxygenase. *Proc. Natl. Acad. Sci. U.S.A.* **2006**, *103*, 9832−9837.

(6) Denisov, I. G.; Makris, T. M.; Sligar, S. G.; Schlichting, I. Structure and Chemistry of Cytochrome P450. *Chem. Rev.* **2005**, *105*, 2253−2278.

(7) Jasniewski, A. J.; Que, L., Jr. Dioxygen Activation by Nonheme Diiron Enzymes: Diverse Dioxygen Adducts, High-Valent Intermediates, and Related Model Complexes. *Chem. Rev.* **2018**, *118*, 2554−2592.

(8) Benkovic, S. J.; Hammes-Schiffer, S. A Perspective on Enzyme Catalysis. *Science* **2003**, *301*, 1196−1202.

(9) Kal, S.; Que, L., Jr Activation of a Non-Heme FeIII-OOH by a Second FeIII to Hydroxylate Strong C−H Bonds: Possible Implications for Soluble Methane Monooxygenase. *Angew. Chen., Int. Ed.* **2019**, *58*, 8484−8488.

(10) Shu, L.; Nesheim, J. C.; Kauffmann, K.; Münck, E.; Lipscomb, J. D.; Que, L. An Fe2IVO2 Diamond Core Structure for the Key Intermediate Q of Methane Monooxygenase. *Science* **1997**, *275*, 515−518.

(11) Acheson, J. F.; Bailey, L. J.; Brunold, T. C.; Fox, B. G. In-crystal reaction cycle of a toluene-bound diiron hydroxylase. *Nature* **2017**, *544*, 191−195.

(12) Dong, J.; Fernández-Fueyo, E.; Hollmann, F.; Paul, C. E.; Pesic, M.; Schmidt, S.; Wang, Y.; Younes, S.; Zhang, W. Biocatalytic Oxidation Reactions: A Chemist's Perspective. *Angew. Chen., Int. Ed.* **2018**, *57*, 9238−9261.

(13) Baik, M.-H.; Newcomb, M.; Friesner, R. A.; Lippard, S. J. Mechanistic Studies on the Hydroxylation of Methane by Methane Monooxygenase. *Chem. Rev.* **2003**, *103*, 2385−2420.

(14) Coggins, M. K.; Toledo, S.; Kovacs, J. A. Isolation and Characterization of a Dihydroxo-Bridged Iron(III,III)(μ-OH)2 Diamond Core Derived from Dioxygen. *Inorg. Chem.* **2013**, *52*, 13325−13331.

(15) Banerjee, R.; Proshlyakov, Y.; Lipscomb, J. D.; Proshlyakov, D. A. Structure of the key species in the enzymatic oxidation of methane to methanol. *Nature* **2015**, *518*, 431−434.

(16) Fukuzumi, S.; Lee, Y.-M.; Jung, J.; Nam, W. Thermal and photocatalytic oxidation of organic substrates by dioxygen with water as an electron source. *Green Chem.* **2018**, *20*, 948−963.

(17) Breslow, R. Artificial Enzymes. *Science* **1982**, *218*, 532−537.

(18) Do, L. H.; Xue, G.; Que, L., Jr.; Lippard, S. J. Evaluating the Identity and Diiron Core Transformations of a (μ-Oxo)diiron(III) Complex Supported by Electron-Rich Tris(pyridyl-2-methyl)amine Ligands. *Inorg. Chem.* **2012**, *51*, 2393−2402.

(19) Guan, H.; Tung, C.-H.; Liu, L. Methane Monooxygenase Mimic Asymmetric Oxidation: Self-Assembling μ-Hydroxo, Carboxylate-Bridged Diiron(III)-Catalyzed Enantioselective Dehydrogenation. *J. Am. Chem. Soc.* **2022**, *144*, 5976−5984.

(20) Ren, X.; Fasan, R. Synergistic catalysis in an artificial enzyme. *Nat. Catal.* **2020**, *3*, 184−185.

(21) Breslow, R. Biomimetic Chemistry and Artificial Enzymes: Catalysis by Design. *Acc. Chem. Res.* **1995**, *28*, 146−153.

(22) Murakami, Y.; Kikuchi, J.-i.; Hisaeda, Y.; Hayashida, O. Artificial Enzymes. *Chem. Rev.* **1996**, *96*, 721−758.

(23) Nam, W.; Oh, S.-Y.; Sun, Y. J.; Kim, J.; Kim, W.-K.; Woo, S. K.; Shin, W. Factors Affecting the Catalytic Epoxidation of Olefins by Iron Porphyrin Complexes and H2O2 in Protic Solvents. *J. Org. Chem.* **2003**, *68*, 7903−7906.

(24) Srinivas, K. A.; Kumar, A.; Chauhan, S. M. S. Epoxidation of alkenes with hydrogen peroxide catalyzed by iron(iii) porphyrins in ionic liquids. *Chem. Commun.* **2002**, *20*, 2456−2457.

(25) Neisen, B. D.; Gagnon, N. L.; Dhar, D.; Spaeth, A. D.; Tolman, W. B. Formally Copper(III)−Alkylperoxo Complexes as Models of Possible Intermediates in Monooxygenase Enzymes. *J. Am. Chem. Soc.* **2017**, *139*, 10220−10223.
(26) Song, Y.; Feng, X.; Lin, W. 9.10 - Metal-Organic Frameworks for Catalytic Applications. In *Comprehensive Coordination Chemistry III*; Constable, E. C., Parkin, G., QueJr, L., Eds.; Elsevier: Oxford, 2021, pp 228−259.
(27) Drake, T.; Ji, P.; Lin, W. Site Isolation in Metal−Organic Frameworks Enables Novel Transition Metal Catalysis. *Acc. Chem. Res.* **2018**, *51*, 2129−2138.
(28) Yaghi, O. M.; Kalmutzki, M. J.; Diercks, C. S. Building Units of MOFs. In *Introduction to Reticular Chemistry*; Wiley, 2019, pp 57−81.
(29) Liu, J.; Chen, L.; Cui, H.; Zhang, J.; Zhang, L.; Su, C.-Y. Applications of metal−organic frameworks in heterogeneous supramolecular catalysis. *Chem. Soc. Rev.* **2014**, *43*, 6011−6061.
(30) Huang, Y.-B.; Liang, J.; Wang, X.-S.; Cao, R. Multifunctional metal−organic framework catalysts: synergistic catalysis and tandem reactions. *Chem. Soc. Rev.* **2017**, *46*, 126−157.
(31) Feng, X.; Song, Y.; Lin, W. Transforming Hydroxide-Containing Metal−Organic Framework Nodes for Transition Metal Catalysis. *Trends Chem* **2020**, *2*, 965−979.
(32) Feng, L.; Wang, K.-Y.; Willman, J.; Zhou, H.-C. Hierarchy in Metal−Organic Frameworks. *ACS Cent. Sci* **2020**, *6*, 359−367.
(33) Syed, Z. H.; Sha, F.; Zhang, X.; Kaphan, D. M.; Delferro, M.; Farha, O. K. Metal−Organic Framework Nodes as a Supporting Platform for Tailoring the Activity of Metal Catalysts. *ACS Catal.* **2020**, *10*, 11556−11566.
(34) Wei, Y.-S.; Zhang, M.; Zou, R.; Xu, Q. Metal−Organic Framework-Based Catalysts with Single Metal Sites. *Chem. Rev.* **2020**, *120*, 12089−12174.
(35) Khan, I. S.; Garzon-Tovar, L.; Mateo, D.; Gascon, J. Metal-Organic-Frameworks and Their Derived Materials in Photo-Thermal Catalysis. *Eur. J. Inorg. Chem.* **2022**, *2022*, No. e202200316.
(36) Feng, X.; Song, Y.; Chen, J. S.; Xu, Z.; Dunn, S. J.; Lin, W. Rational Construction of an Artificial Binuclear Copper Monooxygenase in a Metal−Organic Framework. *J. Am. Chem. Soc.* **2021**, *143*, 1107−1118.
(37) Nath, I.; Chakraborty, J.; Verpoort, F. Metal organic frameworks mimicking natural enzymes: a structural and functional analogy. *Chem. Soc. Rev.* **2016**, *45*, 4127−4170.
(38) Zhao, M.; Ou, S.; Wu, C.-D. Porous Metal−Organic Frameworks for Heterogeneous Biomimetic Catalysis. *Acc. Chem. Res.* **2014**, *47*, 1199−1207.
(39) Li, J.; Huang, H.; Xue, W.; Sun, K.; Song, X.; Wu, C.; Nie, L.; Li, Y.; Liu, C.; Pan, Y.; Jiang, H.-L.; Mei, D.; Zhong, C. Self-adaptive dual-metal-site pairs in metal-organic frameworks for selective CO2 photoreduction to CH4. *Nat. Catal.* **2021**, *4*, 719−729.
(40) Baek, J.; Rungtaweevoranit, B.; Pei, X.; Park, M.; Fakra, S. C.; Liu, Y.-S.; Matheu, R.; Alshmimri, S. A.; Alshehri, S.; Trickett, C. A.; Somorjai, G. A.; Yaghi, O. M. Bioinspired Metal−Organic Framework Catalysts for Selective Methane Oxidation to Methanol. *J. Am. Chem. Soc.* **2018**, *140*, 18208−18216.
(41) Osadchii, D. Y.; Olivos-Suarez, A. I.; Szécsényi, Á.; Li, G.; Nasalevich, M. A.; Dugulan, I. A.; Crespo, P. S.; Hensen, E. J. M.; Veber, S. L.; Fedin, M. V.; Sankar, G.; Pidko, E. A.; Gascon, J. Isolated Fe Sites in Metal Organic Frameworks Catalyze the Direct Conversion of Methane to Methanol. *ACS Catal.* **2018**, *8*, 5542−5548.
(42) Ikuno, T.; Zheng, J.; Vjunov, A.; Sanchez-Sanchez, M.; Ortuño, M. A.; Pahls, D. R.; Fulton, J. L.; Camaioni, D. M.; Li, Z.; Ray, D.; Mehdi, B. L.; Browning, N. D.; Farha, O. K.; Hupp, J. T.; Cramer, C. J.; Gagliardi, L.; Lercher, J. A. Methane Oxidation to Methanol Catalyzed by Cu-Oxo Clusters Stabilized in NU-1000 Metal−Organic Framework. *J. Am. Chem. Soc.* **2017**, *139*, 10294−10301.
(43) Lan, G.; Fan, Y.; Shi, W.; You, E.; Veroneau, S. S.; Lin, W. Biomimetic active sites on monolayered metal−organic frameworks for artificial photosynthesis. *Nat. Catal.* **2022**, *5*, 1006−1018.
(44) Zheng, J.; Ye, J.; Ortuño, M. A.; Fulton, J. L.; Gutiérrez, O. Y.; Camaioni, D. M.; Motkuri, R. K.; Li, Z.; Webber, T. E.; Mehdi, B. L.; Browning, N. D.; Penn, R. L.; Farha, O. K.; Hupp, J. T.; Truhlar, D. G.; Cramer, C. J.; Lercher, J. A. Selective Methane Oxidation to Methanol on Cu-Oxo Dimers Stabilized by Zirconia Nodes of an NU-1000 Metal−Organic Framework. *J. Am. Chem. Soc.* **2019**, *141*, 9292−9304.
(45) Liu, G.; Cui, H.; Wang, S.; Zhang, L.; Su, C.-Y. A series of highly stable porphyrinic metal−organic frameworks based on iron−oxo chain clusters: design, synthesis and biomimetic catalysis. *Journal of Materials Chemistry A* **2020**, *8*, 8376−8382.
(46) Amaro-Gahete, J.; Pavliuk, M. V.; Tian, H.; Esquivel, D.; Romero-Salguero, F. J.; Ott, S. Catalytic systems mimicking the [FeFe]-hydrogenase active site for visible-light-driven hydrogen production. *Coord. Chem. Rev.* **2021**, *448*, 214172.
(47) Castner, A. T.; Johnson, B. A.; Cohen, S. M.; Ott, S. Mimicking the Electron Transport Chain and Active Site of [FeFe] Hydrogenases in One Metal−Organic Framework: Factors That Influence Charge Transport. *J. Am. Chem. Soc.* **2021**, *143*, 7991−7999.
(48) Rodriguez-Gomez, A.; Ould-Chikh, S.; Castells-Gil, J.; Aguilar-Tapia, A.; Bordet, P.; Alrushaid, M. A.; Marti-Gastaldo, C.; Gascon, J. Fe-MOF Materials as Precursors for the Catalytic Dehydrogenation of Isobutane. *ACS Catal.* **2022**, *12*, 3832−3844.
(49) Stanley, P. M.; Su, A. Y.; Ramm, V.; Fink, P.; Kimna, C.; Lieleg, O.; Elsner, M.; Lercher, J. A.; Rieger, B.; Warnan, J.; Fischer, R. A. Photocatalytic CO2-to-Syngas Evolution with Molecular Catalyst Metal-Organic Framework Nanozymes. *Adv. Mater.* **2023**, *35*, 2207380.
(50) Bai, L.; Hsu, C.-S.; Alexander, D. T. L.; Chen, H. M.; Hu, X. Double-atom catalysts as a molecular platform for heterogeneous oxygen evolution electrocatalysis. *Nature Energy* **2021**, *6*, 1054−1066.
(51) Li, L.; Yuan, K.; Chen, Y. Breaking the Scaling Relationship Limit: From Single-Atom to Dual-Atom Catalysts. *Acc. Mater. Res.* **2022**, *3*, 584−596.
(52) Li, L.; Huang, S.; Cao, R.; Yuan, K.; Lu, C.; Huang, B.; Tang, X.; Hu, T.; Zhuang, X.; Chen, Y. Optimizing Microenvironment of Asymmetric N,S-Coordinated Single-Atom Fe via Axial Fifth Coordination toward Efficient Oxygen Electroreduction. *Small* **2022**, *18*, 2105387.
(53) Huang, B.; Huang, S.; Lu, C.; Li, L.; Chen, J.; Hu, T.; Lützenkirchen-Hecht, D.; Yuan, K.; Zhuang, X.; Chen, Y. Decrypting the Influence of Axial Coordination on the Electronic Microenvironment of Co-N5 Site for Enhanced Electrocatalytic Reaction. *CCS Chemistry* **2022**, *0*, 1−12.
(54) Yuan, K.; Lützenkirchen-Hecht, D.; Li, L.; Shuai, L.; Li, Y.; Cao, R.; Qiu, M.; Zhuang, X.; Leung, M. K. H.; Chen, Y.; Scherf, U. Boosting Oxygen Reduction of Single Iron Active Sites via Geometric and Electronic Engineering: Nitrogen and Phosphorus Dual Coordination. *J. Am. Chem. Soc.* **2020**, *142*, 2404−2412.
(55) Bloch, E. D.; Britt, D.; Lee, C.; Doonan, C. J.; Uribe-Romo, F. J.; Furukawa, H.; Long, J. R.; Yaghi, O. M. Metal Insertion in a Microporous Metal−Organic Framework Lined with 2,2′-Bipyridine. *J. Am. Chem. Soc.* **2010**, *132*, 14382−14384.
(56) Yildiz, C.; Kutonova, K.; Oßwald, S.; Titze-Alonso, A.; Bitzer, J.; Bräse, S.; Kleist, W. Post-synthetic Modification of DUT-5-based Metal Organic Frameworks for the Generation of Single-site Catalysts and their Application in Selective Epoxidation Reactions. *ChemCatChem* **2020**, *12*, 1134−1142.
(57) Song, Y.; Feng, X.; Chen, J. S.; Brzezinski, C.; Xu, Z.; Lin, W. Multistep Engineering of Synergistic Catalysts in a Metal−Organic Framework for Tandem C−O Bond Cleavage. *J. Am. Chem. Soc.* **2020**, *142*, 4872−4882.
(58) Feng, X.; Ji, P.; Li, Z.; Drake, T.; Oliveres, P.; Chen, E. Y.; Song, Y.; Wang, C.; Lin, W. Aluminum Hydroxide Secondary Building Units in a Metal−Organic Framework Support Earth-Abundant Metal Catalysts for Broad-Scope Organic Transformations. *ACS Catal.* **2019**, *9*, 3327−3337.
(59) Senkovska, I.; Hoffmann, F.; Fröba, M.; Getzschmann, J.; Böhlmann, W.; Kaskel, S. New highly porous aluminium based metal-

https://doi.org/10.1021/jacs.3c01498
J. Am. Chem. Soc. 2023, 145, 8647−8655

organic frameworks: Al(OH)(ndc) (ndc=2,6-naphthalene dicarboxylate) and Al(OH)(bpdc) (bpdc=4,4′-biphenyl dicarboxylate). *Microporous Mesoporous Mater.* **2009**, *122*, 93−98.
(60) Randall, C. R.; Shu, L.; Chiou, Y.-M.; Hagen, K. S.; Ito, M.; Kitajima, N.; Lachicotte, R. J.; Zang, Y.; Que, L., Jr. X-ray Absorption Pre-Edge Studies of High-spin Iron(II) Complexes. *Inorg. Chem.* **1995**, *34*, 1036−1039.
(61) Rudd, D. J.; Sazinsky, M. H.; Lippard, S. J.; Hedman, B.; Hodgson, K. O. X-ray Absorption Spectroscopic Study of the Reduced Hydroxylases of Methane Monooxygenase and Toluene/o-Xylene Monooxygenase: Differences in Active Site Structure and Effects of the Coupling Proteins MMOB and ToMOD. *Inorg. Chem.* **2005**, *44*, 4546−4554.
(62) Sarangi, R. X-ray absorption near-edge spectroscopy in bioinorganic chemistry: Application to M−O2 systems. *Coord. Chem. Rev.* **2013**, *257*, 459−472.
(63) Westre, T. E.; Kennepohl, P.; DeWitt, J. G.; Hedman, B.; Hodgson, K. O.; Solomon, E. I. A Multiplet Analysis of Fe K-Edge 1s → 3d Pre-Edge Features of Iron Complexes. *J. Am. Chem. Soc.* **1997**, *119*, 6297−6314.
(64) Hadjiivanov, K. I.; Panayotov, D. A.; Mihaylov, M. Y.; Ivanova, E. Z.; Chakarova, K. K.; Andonova, S. M.; Drenchev, N. L. Power of Infrared and Raman Spectroscopies to Characterize Metal-Organic Frameworks and Investigate Their Interaction with Guest Molecules. *Chem. Rev.* **2021**, *121*, 1286−1424.
(65) Devic, T.; Horcajada, P.; Serre, C.; Salles, F.; Maurin, G.; Moulin, B.; Heurtaux, D.; Clet, G.; Vimont, A.; Grenèche, J.-M.; Ouay, B. L.; Moreau, F.; Magnier, E.; Filinchuk, Y.; Marrot, J.; Lavalley, J.-C.; Daturi, M.; Férey, G. Functionalization in Flexible Porous Solids: Effects on the Pore Opening and the Host−Guest Interactions. *J. Am. Chem. Soc.* **2010**, *132*, 1127−1136.
(66) Punniyamurthy, T.; Velusamy, S.; Iqbal, J. Recent Advances in Transition Metal Catalyzed Oxidation of Organic Substrates with Molecular Oxygen. *Chem. Rev.* **2005**, *105*, 2329−2364.
(67) Parmeggiani, C.; Cardona, F. Transition metal based catalysts in the aerobic oxidation of alcohols. *Green Chem.* **2012**, *14*, 547−564.
(68) Chandra, A.; Ansari, M.; Monte-Pérez, I.; Kundu, S.; Rajaraman, G.; Ray, K. Ligand-Constraint-Induced Peroxide Activation for Electrophilic Reactivity. *Angew. Chen., Int. Ed.* **2021**, *60*, 14954−14959.
(69) Ambundo, E. A.; Friesner, R. A.; Lippard, S. J. Reactions of Methane Monooxygenase Intermediate Q with Derivatized Methanes. *J. Am. Chem. Soc.* **2002**, *124*, 8770−8771.

https://doi.org/10.1021/jacs.3c01498
J. Am. Chem. Soc. 2023, 145, 8647−8655